FEATURE ARTICLE

Unravelling the Origin of Intermolecular Interactions Using Absolutely Localized Molecular Orbitals

Rustam Z. Khaliullin,*,†,‡ Erika A. Cobar,‡,§ Rohini C. Lochan,†,‡ Alexis T. Bell,†,¶ and Martin Head-Gordon*,†,‡

Chemical Sciences Division, Lawrence Berkeley National Laboratory, Berkeley, California 94720, Department of Chemistry, University of California, Berkeley, California 94720, Laboratory of Computational Biology, Computational Biophysics Section, Heart, Lung, and Blood Institute, National Institutes of Health, Bethesda, Maryland 20892, and Department of Chemical Engineering, University of California, Berkeley, California 94720

Received: May 14, 2007; In Final Form: July 3, 2007

An energy decomposition analysis (EDA) method is proposed to isolate physically relevant components of the total intermolecular interaction energies such as the contribution from interacting frozen monomer densities, the energy lowering due to polarization of the densities, and the further energy lowering due to charge-transfer effects. This method is conceptually similar to existing EDA methods such as Morokuma analysis but includes several important new features. The first is a fully self-consistent treatment of the energy lowering due to polarization, which is evaluated by a self-consistent field calculation in which the molecular orbital coefficients are constrained to be block-diagonal (absolutely localized) in the interacting molecules to prohibit charge transfer. The second new feature is the ability to separate forward and back-donation in the charge-transfer energy term using a perturbative approximation starting from the optimized block-diagonal reference. The newly proposed EDA method is used to understand the fundamental aspects of intermolecular interactions such as the degree of covalency in the hydrogen bonding in water and the contributions of forward and back-donation in synergic bonding in metal complexes. Additionally, it is demonstrated that this method can be used to identify the factors controlling the interaction of the molecular hydrogen with open metal centers in potential hydrogen storage materials and the interaction of methane with rhenium complexes.

1. Introduction

Intermolecular interactions determine physical and chemical properties of a broad class of important systems such as liquids, solutions, and molecular solids. They control self-assembly and self-organization processes in supramolecular polymers, liquid crystals, and other supramolecular systems.[1,2] Hydrogen bonding, one of the most abundant types of intermolecular interactions, plays an important role in the chemistry of numerous systems, ranging from small water clusters to bulk water, as well as solvated biomolecules.[3−5] Metal−ligand interactions give rise to a wide variety of metal complexes with different physical properties, different chemical behavior, and numerous practical applications.[6,7] Many catalyzed reactions involve nondissociative molecular adsorption, formation of σ-complexes, and solvent−active site interactions.[8−10] These interactions direct catalyzed chemical processes and often determine activity and selectivity of catalysts.

The strength of intermolecular binding is inextricably connected to the fundamental nature of interactions between the molecules.[11] Intermolecular complexes can be stabilized through weak dispersive forces, electrostatic effects (for example charge−charge, charge−dipole, and charge−induced dipole interactions) and donor−acceptor type orbital interactions such as forward and back-donation of electron density between the molecules. Depending on the extent of these interactions, the intermolecular binding could vary in strength from just several kJ/mol (Van der Waals complexes) to several hundred kJ/mol (metal−ligand bonds in metal complexes). Understanding the contributions of various interaction modes enables one to tune the strength of the intermolecular binding to the ideal range by designing materials that promote desirable effects.

Because of the broad importance of intermolecular interactions, there is considerable interest in developing theoretical approaches for describing intermolecular interactions. One of the most powerful techniques that modern first principles electronic structure methods provide to study and analyze the nature of intermolecular interactions is the decomposition of the total molecular binding energy into the physically meaningful components such as dispersion, electrostatic, polarization, charge-transfer, and geometry relaxation terms.[12−24] Such energy decomposition schemes help provide insights into the nature and mechanisms of molecular interactions and, thus, aid the design of materials that possess desired interactions. Energy decomposition analysis (EDA) is also a useful tool in developing reliable force fields for condensed phase molecular simula-

* Corresponding authors. E-mail: R.Z.K., rustam@khaliullin.com; M.H.-G., mhg@bastille.cchem.berkeley.edu.
† Lawrence Berkeley National Laboratory.
‡ Department of Chemistry, University of California, Berkeley.
§ National Institutes of Health.
¶ Department of Chemical Engineering, University of California, Berkeley.

10.1021/jp073685z CCC: $37.00
Published on Web 07/27/2007

Rustam Z. Khaliullin earned his M.S. with Highest Honors in Chemistry from the Higher Chemical College of the Russian Academy of Sciences in 2002. He pursued graduate studies at the University of California, Berkeley, working jointly with Prof. Martin Head-Gordon and Prof. Alexis T. Bell. He received a Ph.D. in Theoretical Chemistry in 2007. His graduate research has focused on the development of ab initio electronic structure methods for intermolecular interactions and application of ab initio methods to catalytic reactions.

Erika A. Cobar earned her B.S. with Highest Honors in Chemistry in 2003 from the University of California, Davis. She is now a graduate student in the Chemistry department at the University of California, Berkeley, working jointly in the groups of Prof. Martin Head-Gordon and Prof. Robert G. Bergman. Erika is presently working as a research fellow in the Computational Biophysics Section of the Laboratory of Computational Biology at the National Institutes of Health, National Heart, Lung, and Blood Institute in Bethesda, MD, under the direction of Dr. Bernard R. Brooks. Her research focuses on the elucidation of reaction mechanisms in organometallic and bioinorganic chemistry, using both QM and QM/MM methods.

Rohini C. Lochan recieved her (Integrated) M.S. degree in Chemistry from the Indian Institute of Technology, Bombay, in 2002. She graduated with a Ph.D. in Chemistry from the University of California, Berkeley, in 2006 where she worked under the supervision of Prof. Martin Head-Gordon. She is currently working as a consultant at Q-Chem, Inc., in Pittsburgh. Her research interests include development of fast and accurate electronic structure methods and study of the fundamental interactions of molecular hydrogen with potential hydrogen storage materials.

Alexis T. Bell received his Sc.D. degree from the Massachusetts Institute of Technology in Chemical Engineering in 1967. That same year he joined the Department of Chemical Engineering at the University of California at Berkeley, where he currently holds the title of Full Professor. He is also a Faculty Senior Scientist in the Lawrence Berkeley National Laboratory. Prof. Bell is known for his research in the field of heterogeneous catalysis and is recognized as one of the leaders in applying in situ spectroscopic techniques in combination with isotopic tracer techniques to the study of catalyzed reactions. He has been involved, as well, in the development and application of theoretical techniques for understanding the relationships between catalyst structure and the dynamics of elementary processes at a fundamental level.

Martin Head-Gordon obtained his Ph.D. degree from Carnegie-Mellon University in 1989, studying with John Pople. After postdoctoral study with John Tully at Bell Laboratories, he took up a position in the Chemistry Department at the University of California, Berkeley, where he is now Professor, with a joint appointment in the Chemical Sciences Division of Lawrence Berkeley National Laboratory. His research interests focus on electronic structure theory and algorithms.

tions.[25−32] EDA has the ability to measure the effect of functional group substitution on the intermolecular binding energies and can be used in combinatorial drug design and for building QSAR models.

The need for physically reasonable and quantitatively useful values of the intermolecular interaction energy components has resulted in numerous decomposition schemes proposed since the early years of theoretical chemistry.[12−24] Two main approaches are available for the decomposition of the interaction energy. The first relies on symmetry-adapted perturbation theory (SAPT)[12,13] and is becoming widely used because of the recently developed ability[33,34] to use inexpensive density functional theory in the analysis. The second approach to decomposing interaction energies is variational.[14−22] In this paper, we are concerned primarily with variational self-consistent field approaches because they are computationally faster than perturbation methods and produce meaningful results for strongly interacting systems for which the perturbation approach fails.

Most variational methods represent the total interaction energy as a sum of a frozen density interaction energy, a polarization energy, and charge-transfer energy terms. The frozen density term is calculated as the interaction energy of the unrelaxed electron densities on the molecules. The polarization term is due to the deformation (or polarization) of the electron clouds of the molecules in the field of each other. Quantum mechanically, it can be described as the energy lowering due to the intramolecular relaxation of the molecular orbitals. It is worth mentioning that the polarization energy term obtained with variational methods is defined differently from the polarization terms in SAPT, where it also implicitly includes dispersion in addition to induction. Finally, the charge transfer can be pictured as the electron flow to and from each molecule in the system and it is described by the intermolecular relaxation (or mixing) of the molecular orbitals. For instance, the ionic bonding can be described in terms of just the frozen density and polarization interactions. The amount of the electron transfer or charge transfer between the molecules is often viewed as a measure of covalency of a chemical bond.

The method of Kitaura and Morokuma (KM) is the most widely used variational energy decomposition method.[14,16] In this approach, the energy components are calculated by setting certain elements of the effective Hamiltonian to zero. It has been shown that the improper antisymmetrization of the intermediate wavefunctions used to evaluate the polarization and the charge-transfer terms in KM method can result in numerical instabilities of these components at short distances and with large basis sets.[35−37] Moreover, the residual coupling terms introduced as a correction to reproduce the total interaction energy do not have clear physical interpretation and in some cases can be of the order of the legitimate terms.[38,39] Despite these limitations the KM EDA has been widely and successfully applied to molecular complexes of various types.[40−42]

Several alternative schemes have been proposed to avoid problems of the KM EDA. Most popular of these are the restricted variational space (RVS) analysis,[15,16] the constrained space orbital variations (CSOV),[17,18] and the natural energy decoposition analysis (NEDA).[19−21] The CSOV and a closely related method, RVS, are perhaps the best modifications of the KM method. They use fully antisymmetrized wavefunctions to calculate all intermediate energies and, therefore, avoid the short-range problems of the KM procedure. Like the KM method, the CSOV and RVS schemes are nonadditive, but the missing components are generally small. Nevertheless, they do not produce a self-consistent polarization energy nor do they separate the polarization term from the charge-transfer term completely. Lack of self-consistency in the polarization and charge-transfer components is the reason for nonadditivity and order-of-the-fragment dependence in these schemes. NEDA does not obtain the intermediate wavefunctions variationally, and therefore, the resulting polarization terms can be underestimated, whereas the charge-transfer terms can be overestimated.

Most of the formal and practical problems with the existing decomposition schemes stem from the inability to determine the intermediate self-consistent energy corresponding to the variationally optimized properly antisymmetrized many-electron wavefunction constructed from MOs fully localized on the molecules. In this paper, we present an energy decomposition method based on absolutely localized molecular orbitals[43−47] that calculates the self-consistent variational polarization energy and, therefore, naturally separates the polarization energy term from the charge-transfer term. Due to its variational nature, this decomposition method can be applied to both strongly and weakly interacting molecules. We also show that the absolutely localized molecular orbital formulation can be used to further

separate the charge-transfer term into bonding and back-bonding components.

To demonstrate the validity and usefulness of the new EDA based on the absolutely localized molecular orbitals (ALMO EDA), we applied it to a series of problems of chemical interest:

- covalency of hydrogen bonding in the water dimer
- solvation of alkali cations in small water clusters
- donor−acceptor interactions in borane adducts
- synergic bonding in Zeise's salt and its analogs
- interaction of molecular hydrogen with transition metal centers
- interaction of methane with (η^6-R-C_5H_4)Re(CO)$_2$ complexes

For the first four systems, the bonding mechanisms are relatively well understood and we show that the ALMO EDA results are consistent with existing conceptual description of intermolecular bonding. The last two examples demonstrate that the ALMO EDA can assist in solving practical chemical problems. The systems considered here are related to the design of effective hydrogen fuel storage materials and the catalytic activation of carbon−hydrogen bonds in alkanes.

2. Theory

The ALMO energy decomposition analysis was implemented in the Q-Chem software package.[48] Absolutely localized molecular orbitals have been originally used to speed up evaluation of the SCF energies for large ensembles of molecules.[43] Unlike conventional MOs, which are generally delocalized over all molecules in the system, the absolutely localized molecular orbitals (ALMOs) are expanded in terms of the atomic orbitals (AOs) of only a given molecule.[43,44,46,47] Such an expansion excludes charge transfer from one molecule to another in a natural way. The ALMOs are not orthogonal from one molecule to the next and, therefore, both the construction of a properly antisymmetrized many-electron wavefunction and the minimization of the electronic energy as a function of the ALMO coefficients differ from conventional SCF methods. The self-consistent field procedure for the variational optimization of the nonorthogonal ALMOs is called SCF for molecular interactions, or SCF MI.[43,46,47] Mathematical details of the SCF MI method are given elsewhere.[43] The variationally optimized ALMOs represent the intermediate many-electron state with no electron flow between the molecules, thus enabling an elegant separation of the polarization from the charge-transfer terms. In this section, we will describe how the absolutely localized orbitals and the SCF MI can be used in an energy decomposition scheme.

The overall binding energy is decomposed into the geometric distortion (GD), the frozen density component (FRZ), the polarization (POL), and the charge-transfer (CT) terms.

$$\Delta E_{\mathrm{BIND}} = \Delta E_{\mathrm{GD}} + \Delta E_{\mathrm{FRZ}} + \Delta E_{\mathrm{POL}} + \Delta E_{\mathrm{CT}} \qquad (1)$$

The first step, ΔE_{GD}, is the energy penalty associated with geometric distortion of the isolated molecules from their optimized geometry to the geometry that they have in the complex.

The frozen density term (FRZ) is defined as the SCF energy change that corresponds to bringing infinitely separated distorted molecules into the complex geometry without any relaxation of the MOs on the fragments.

$$\Delta E_{\mathrm{FRZ}} \equiv E_{\mathrm{scf}}(\Psi_0) - \sum_x E_{\mathrm{scf}}(\Psi_x) \qquad (2)$$

$E_{\mathrm{scf}}(\Psi_x)$ is the SCF energy of the fully optimized wavefunction of the isolated molecule x with its nuclei fixed at the complex geometry and Ψ_0 is the properly antisymmetrized many-electron wavefunction of the supermolecule constructed from the unrelaxed nonorthogonal occupied MOs of the fragments. The frozen density term is sometimes represented as a sum of two terms: (a) a Coulomb (ELS) term and (b) an exchange term in the HF theory (EX) or an exchange-correlation term in the Kohn−Sham theory (XC). These two contributions are well-defined, but

$$\Delta E_{\mathrm{FRZ}} = \Delta E_{\mathrm{ELS}} + \Delta E_{\mathrm{EX/XC}} \qquad (3)$$

because they correspond to the energy of wavefunctions that are not properly antisymmetrized, we will not separate them.

The polarization energy is defined as the energy lowering due to intramolecular relaxation of each molecule's absolutely localized MOs in the field of all other molecules in the system. The intramolecular relaxation is constrained to include only variations that keep MOs localized on their molecule. The ALMO expansion thus explicitly excludes charge transfer from one molecule to another and the variational optimization of the ALMOs performed in the SCF MI method is, therefore, an ideal method for calculating the polarization term.

$$\Delta E_{\mathrm{POL}} \equiv E_{\mathrm{scf}}(\Psi_{\mathrm{ALMO}}) - E_{\mathrm{scf}}(\Psi_0) \qquad (4)$$

Ψ_{ALMO} is a determinant constructed from the fully optimized ALMOs.

It is important to note that this definition of the ALMOs and thus polarization energy relies on an underlying basis set that is partitioned among the fragments. AO basis sets are ideal in this regard and give well-defined polarization energies as long as there are no linear dependences. In the linearly dependent limit where basis functions on one fragment can exactly mimic functions on another fragment this ceases to be the case.[15] For the AO basis sets used routinely in quantum chemistry, this is not an issue.

The remaining portion of the total interaction energy, the charge-transfer (CT) energy term, is calculated as the counterpoise corrected energy difference between the state formed from the fully relaxed ALMOs, Ψ_{ALMO}, and the state constructed from the fully optimized delocalized MOs, Ψ.

$$\Delta E_{\mathrm{CT}} \equiv E_{\mathrm{scf}}(\Psi) - E_{\mathrm{scf}}(\Psi_{\mathrm{ALMO}}) + \Delta E_{\mathrm{BSSE}} \qquad (5)$$

ΔE_{BSSE} is the (always positive) counterpoise correction that accounts for the basis set superposition error (BSSE). For a detailed discussion of the counterpoise correction methods,[49] see the Appendix. The BSSE is not introduced when calculating frozen density and polarization energy contributions because constrained MO optimization prevents electrons on one molecule from borrowing the AOs of other molecules to compensate for incompleteness of their own AOs. However, the BSSE enters the charge-transfer contribution because both the BSSE and charge transfer result from the same physical phenomenon of delocalization of fragment MOs. Therefore, these terms are inseparable from each other when finite basis sets are used to describe fragments at finite spatial separation. It has been demonstrated that the BSSE decreases faster than charge-transfer effects with the quality of the basis set.[43,50,51] Therefore, the use of medium and large localized Gaussian basis sets (without linear dependencies) make the BSSE component of the interaction energy negligibly small but the charge-transfer component is still nonzero.

ΔE_{CT} defined in eq 5 includes the energy lowering due to electron transfer from occupied orbitals on one molecule to

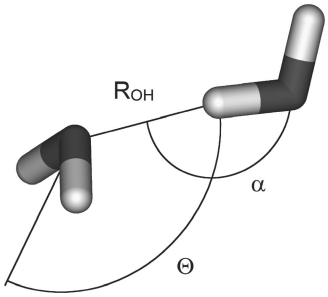

Figure 1. Relative position of the water molecules in the water dimer.

virtual orbitals of another molecule as well as the further energy change caused by induction that accompanies such an occupied-virtual mixing. The energy lowering of the occupied-virtual excitations can be described with a single non-iterative Roothaan step (RS) correction starting from the converged ALMO solution.[43] Most importantly for our present purpose, the mathematical form of the SCF MI(RS) energy expression (see the Appendix) allows one to decompose the occupied-virtual-mixing term into bonding and back-bonding components for each pair of molecules in the complex.

$$\Delta E_{\mathrm{CT}} = \Delta E_{\mathrm{CT}}^{\mathrm{RS}} + \Delta E_{\mathrm{CT}}^{\mathrm{HO}} = \sum_{x,y<x} \{\Delta E_{x\rightarrow y}^{\mathrm{RS}} + \Delta E_{y\rightarrow x}^{\mathrm{RS}}\} + E_{\mathrm{CT}}^{\mathrm{HO}} \quad (6)$$

Thus, the charge-transfer energy term lowering is divided into a contribution from the single noniterative Roothaan step and higher order (HO) relaxation effects. The latter includes all induction effects that accompany occupied-virtual charge transfer and is generally small. The RS contribution divides naturally into forward and back-donation, but the higher order term does not. The BSSE associated with each forward and back-donation term can be corrected individually (see the Appendix).

3. Applications

3.1. Water Dimer. The water dimer is one of the most extensively studied intermolecular complexes.[52−59] Despite the large amount of theoretical and experimental work, the physical nature of hydrogen bonding in the water dimer is still a matter of discussion. The main controversy concerns the amount of charge transfer, i.e., interfragment covalency, in the hydrogen bonding.[58−62] The KM, RVS, and CSOV decomposition methods estimate charge-transfer contribution to be smaller than 20% of the overall Hartree−Fock interaction energy.[15,16,63] According to the NBO-based methods, the charge-transfer energy lowering is significantly larger than the total interaction energy and accounts for around 45% of the intermolecular stabilization energy.[19−21] Accurate separation of the polarization term from the charge-transfer term is essential for determining the amount of covalency in the hydrogen bonding. The polarization and charge-transfer terms defined in this work are detemined variationally from fully antisymmetrized wavefunctions. This feature makes the ALMO EDA an ideal method for studying the nature of the hydrogen bonding.

The water dimer geometry with a C_s symmetry was optimized at the MP2/aug-cc-pVQZ level. Relative position of the molecules in the C_s dimer is described by three parameters shown in Figure 1. The MP2/aug-cc-pVQZ structure is characterized by $\alpha = 171.6°$, $\Theta = 126.8°$, and $R_{\mathrm{OH}} = 1.936$ Å.

The results of the energy decomposition analysis are presented in Table 1. Table 1 shows that the total interaction energies as well as the energy components rapidly converge as the basis set becomes locally complete indicating stability of the proposed decomposition method. Decomposition of the Hartree−Fock energy produces results similar to the KM-type methods but gives a somewhat larger charge-transfer contribution. According to our EDA, charge transfer accounts for 27% of the total hydrogen-bonding energy. When Kohn−Sham DFT is used instead of the Hartree−Fock method (Table 1), all energy terms change because of modification of the exchange and addition of the correlation terms into the mean-field Hamiltonian. The delocalization effect becomes more pronounced for the density functional methods and in some cases the charge-transfer term is more than 50% of the overall binding energy. This observation is consistent with the tendency of the modern density functionals to underestimate the HOMO−LUMO gap[64] which, in the water dimer case, manifests itself in a large charge-transfer energy.

The Hartree−Fock frozen density and polarization energies are comparable to the charge-transfer term. Thus, the interaction energy is equally distributed among three energy terms in the water dimer at the gas-phase equilibrium geometry. However, the relative contribution of the terms varies strongly with the position of the molecules in the dimer. Figure 2 shows the dependence of the HF/aug-cc-pVQZ BSSE corrected energy and its ALMO decomposition on the orientation of the water molecules (Θ is varied and all other internal coordinates remain fixed at their MP2/aug-cc-pVQZ values). The frozen density component increases significantly and becomes repulsive as the O−H bonds of two molecules get closer. At the same time, stabilization due to charge transfer increases upon the closer contact but not strongly enough to compensate for the electron density repulsion. The polarization component does not depend noticeably on the orientation of the molecules in the dimer for the studied range of Θ. The charge-transfer and the polarization terms decrease rapidly with the intermolecule distance (Figure 3) and, at $R_{\mathrm{OH}} > 3$ Å, the interaction energy can be accurately approximated by the frozen density term alone.

The results of the RS perturbative treatment of the charge-transfer term are very close to the exact terms obtained variationally, the difference between them is less than 1 kJ/mol for all methods and basis sets (Table 1). The BSSE calculated perturbatively is also almost identical to the variational BSSE. As expected, the charge transfer occurs mostly from the proton acceptor to the proton donor (95% of the total charge-transfer energy lowering). These results confirm the applicability of the SCF MI(RS) method to systems with hydrogen bonding.

To estimate the energy of geometrical distortion of the molecules in the dimer, we optimized the geometry of the isolated molecules. Because geometry relaxation of the monomers was performed with MP2/aug-cc-pVQZ method, ΔE_{GD} calculated with the density functionals is not necessarily negative. However, small values of ΔE_{GD} for all methods (Table 1) indicate that geometrical distortion of water molecules is insignificant in the water dimer.

Although HF and DFT methods disagree quantitatively on the exact contribution of charge transfer into the intermolecular interaction in the water dimer, it is obvious that its role in hydrogen bonding is not less significant than those of polarization and frozen density interactions. The widespread DFT results indicate that a better description of the intermolecular correlation energy is necessary for the water dimer. ALMOs can be used to extend the energy decomposition analysis beyond the mean-field methods and provide an accurate description of the correlation energy at the MP2 or coupled-cluster levels. This is a problem we hope to report on in the future.

TABLE 1: EDA Results for Water Dimer (kJ/mol) for Geometry Optimized at the MP2/aug-cc-pVQZ Level

exchange:	HF			B3			PW91			B		
correlation:	NONE			LYP			PW91			P86		
X:[a]	D	T	Q	D	T	Q	D	T	Q	D	T	Q
ΔE_{FRZ}	−5.9	−5.2	−4.9	−5.5	−5.4	−5.1	−9.3	−8.7	−8.3	−2.0	−1.9	−1.6
ΔE_{POL}	−4.8	−5.9	−6.0	−4.4	−6.1	−6.5	−2.8	−4.8	−5.2	−4.3	−6.4	−7.0
$\Delta E^{RS}_{D\rightarrow A}$	−0.2	−0.2	−0.2	−0.2	−0.4	−0.3	−0.3	−0.4	−0.4	−0.2	−0.4	−0.3
$\Delta E^{RS}_{A\rightarrow D}$	−3.2	−3.0	−3.3	−7.9	−6.6	−6.7	−10.4	−8.3	−8.3	−10.4	−8.3	−8.3
ΔE^{HO}_{CT}	−0.8	−0.6	−0.6	−0.5	−0.4	−0.3	0.6	0.2	0.0	0.1	0.0	0.0
$\Delta E_{GD}(D)$[b]	0.6	0.7	0.7	−0.2	0.3	−0.0	−0.4	0.1	−0.2	−0.4	0.1	−0.2
$\Delta E_{GD}(A)$[b]	0.1	0.1	0.1	−0.1	−0.2	−0.1	−0.2	−0.2	−0.2	−0.2	−0.2	−0.2
ΔE_{BIND}[c]	**−14.2**	**−14.1**	**−14.2**	**−18.8**	**−18.7**	**−19.0**	**−22.8**	**−22.1**	**−22.5**	**−17.3**	**−17.1**	**−17.6**
ΔE_{BSSE}	1.1	0.3	0.1	0.9	0.2	0.1	1.0	0.2	0.1	0.9	0.1	0.1
ΔE^{RS}_{BSSE}	0.9	0.3	0.1	0.9	0.2	0.1	0.9	0.2	0.1	0.9	0.1	0.1

[a] Basis set used for the EDA is aug-cc-pVXZ. [b] D and A stand for proton-donor and proton-acceptor, respectively. ΔE_{GD} terms calculated with the MP2/aug-cc-pVQZ method for D and A are 0.20 and 0.01 kJ/mol, respectively. [c] BSSE-corrected and uncorrected MP2 total interaction energies are −18.3 and −22.3 kJ/mol for aug-cc-pVDZ, respectively; −19.8 and −23.7 kJ/mol for aug-cc-pVTZ, respectively; and −20.6 and −22.0 kJ/mol for aug-cc-pVQZ, respectively.

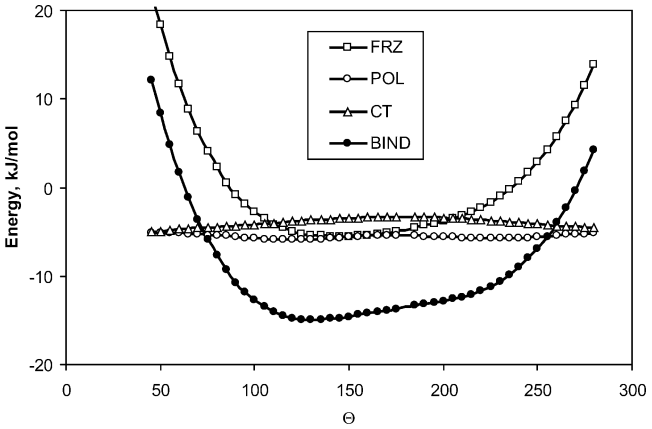

Figure 2. Dependence of the energy components on the relative orientation of the water molecules in the dimer. HF/aug-cc-pVQZ.

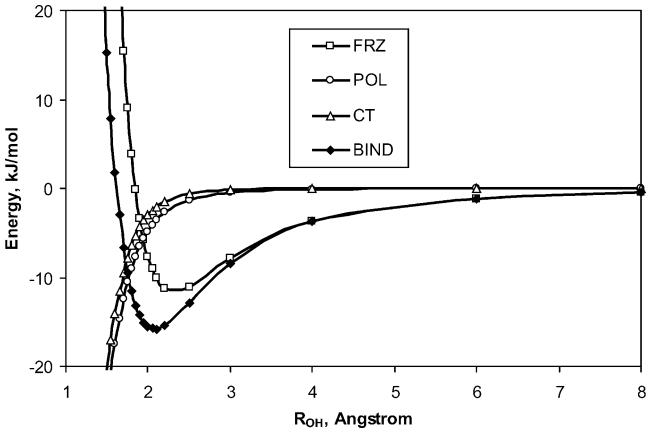

Figure 3. Dependence of the energy components on the distance between the water molecules in the dimer. HF/aug-cc-pVQZ.

3.2. $M(H_2O)_n^+$ Clusters (M = Li, Na, K, Cs, Rb). The local environment of solvated alkali metal ions is an important subject in aqueous chemistry as well as in biology. In this connection, a large number of experimental and theoretical studies have been carried out on the solvation of monovalent cations in small water clusters, showing that smaller cations bind water more strongly than larger cations.[52,65−67] This trend can be qualitatively explained using Pearson's hard soft acid base (HSAB) principle[68,69] according to which the water molecule (a hard Lewis base) interacts preferentially with hard acids (small cations). The cation−water binding in small clusters is described as electrostatic in nature; however, some cation−water bonds are regarded to have a significant covalent contribution. Energy decomposition analysis can provide a quantitative measure of covalency in the cation-water bonding by estimating ΔE_{CT}.

We compare results of the ALMO EDA for cation-water interactions in Li^+, Na^+, K^+, Cs^+, and Rb^+ clusters with one and four water molecules. Geometry optimization and EDA calculations were performed using the BP86 density functional with the aug-cc-pVDZ basis set for O, H atoms and the SRSC pseudopotential basis set for the metal atoms. The results are summarized in Figure 4 (see also Table S1 in the Supporting Information).

For complexes with one water molecule, $M(H_2O)^+$, the largest binding energy is observed for Li^+. The absolute value of ΔE_{BIND} decreases from 135 to 45 kJ/mol in the series from Li^+ to Cs^+. The frozen density interaction is the dominant contribution to the binding between the cation and the water molecule, which indicates that the electrostatic interaction of the positively charged ion with the water dipole is indeed the major component in these interactions. Polarization effects are significantly smaller, but they also play an important role in the binding (the largest contribution of 34% of the total interaction energy is observed for Li^+). Absolute values of both ΔE_{FRZ} and ΔE_{POL} decrease as the M−O distance grows from Li^+ to Cs^+. Charge transfer is noticeable only for lithium−water interactions (8% of the total interaction energy), and it is negligible for all other cations. The single Roothaan step can reproduce such small charge-transfer effects very well (the higher order relaxation term is less than 0.05 kJ/mol). As expected, the electrons are transferred from the water molecule to the cation.

The same trends are observed for interaction of a water molecule with the partially solvated alkali cations $M(H_2O)_3^+$. The interaction energy and its components are smaller in magnitude compared to the energetics of interaction with bare cations (Figure 4). The electric field of $M(H_2O)_3^+$ felt by the fourth water molecule is weaker compared to the electric field of M^+ because of better charge delocalization in the former. This is the reason for the decrease in ΔE_{FRZ} and ΔE_{POL}. Charge transfer from the water molecule to the partially solvated cation is smaller than charge transfer to the bare cation. This is because the cation's electron deficiency is partially compensated in $M(H_2O)_3^+$ by the electron donation from the three neighboring water molecules. The energy of geometrical distortion of the water molecules in the lithium complexes is less than 0.15 kJ/mol and even smaller for all other cations (less than 0.03 kJ/mol).

3.3. Donor−Acceptor Interactions in $H_3B{-}NH_3$, $H_3B{-}CO$, $H_3B{-}N_2$, and $H_3B{-}CN^-$. Donor−acceptor bonding is a

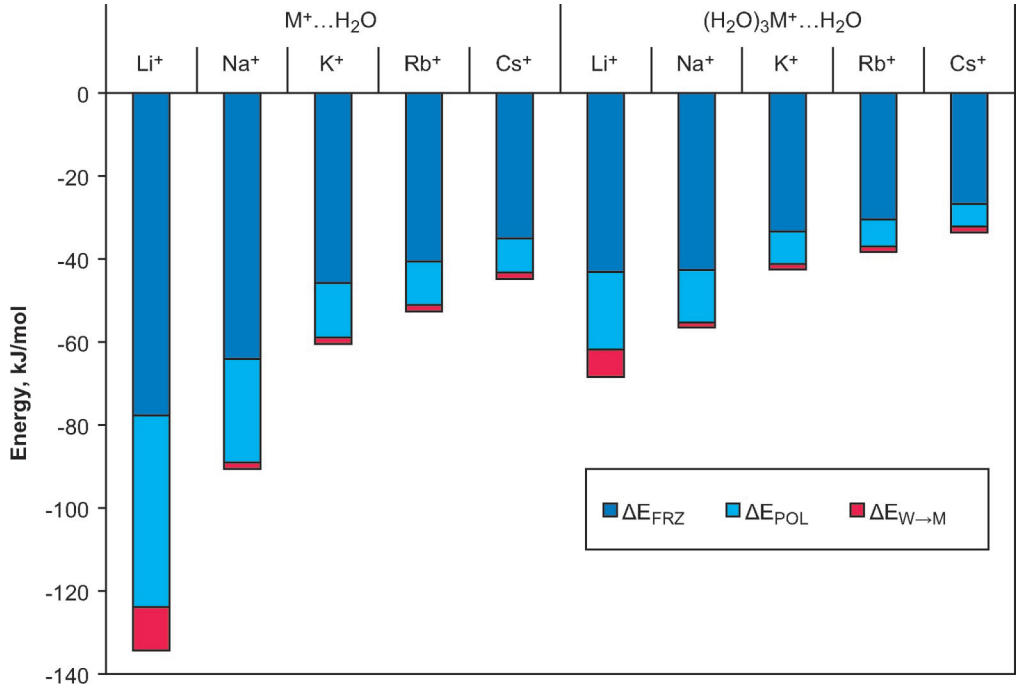

Figure 4. BP86/SRSC/aug-cc-pVDZ EDA results for $M(H_2O)_n^+$ clusters.

TABLE 2: B3LYP/6-31(+,+)G(d,p) EDA Results (kJ/mol) for H_3B-NH_3, H_3B-CO, H_3B-N_2, and H_3B-CN^-

	B−X			
	H_3B-NH_3	H_3B-CO	H_3B-N_2	H_3B-CN^-
ΔE_{FRZ}	103.3	316.7	268.4	184.8
ΔE_{POL}	−127.6	−203.1	−140.4	−306.7
$\Delta E^{RS}_{X\rightarrow B}$	−137.3	−146.1	−110.0	−183.7
$\Delta E^{RS}_{B\rightarrow X}$	−10.7	−136.5	−83.5	−34.1
ΔE^{HO}_{CT}	0.4	0.5	−8.8	−0.8
$\Delta E_{GD}(BH_3)$	54.4	54.7	44.1	91.0
$\Delta E_{GD}(X)$	0.0	0.1	0.1	0.7
ΔE_{BIND}	**−117.5**	**−113.8**	**−30.1**	**−248.8**
ΔE_{BSSE}	6.1	3.3	3.7	3.1
ΔE^{RE}_{BSSE}	5.8	3.2	3.5	3.0
d, Å	1.67	1.53	1.56	1.59

central concept in chemistry.[68,70,71] It is usually represented as donation of a lone electron pair of a Lewis base into an empty orbital of a Lewis acid. The N−B bond in ammonia borane (H_3B-NH_3) is a textbook example of donor−acceptor bonding. This bond has been the subject of numerous experimental and theoretical studies confirming that the electronic structure of ammonia borane is indeed correctly described by its Lewis structure.[19,72−75] The photoelectron spectra[72,73] and EDA studies[19,74−77] of another borane compound, H_3B-CO, suggest that the donor−acceptor bonding in this complex has more complicated character with significant contribution of back-donation of the electron density from BH_3 to CO. We apply the ALMO energy decomposition to analyze and compare the donor−acceptor bonding in H_3B-NH_3 and H_3B-CO complexes. We also compare H_3B-CO to the isoelectronic complexes H_3B-N_2 and H_3B-CN^-.

B3LYP density functional theory with the 6-31(+,+)G(d,p) basis set was used to obtain both the complex geometries and the interaction energy components (Table 2). The energy profiles in Figure 5 were generated by varying the intermolecular distance with all other geometric parameters fixed. Although the total interaction energies are approximately the same for H_3B-NH_3 and H_3B-CO at the equilibrium geometry, the energy components differ significantly (Table 2). The frozen density repulsion is considerably stronger in borane carbonyl for all distances (Figure 5A). The intramolecular orbital relaxation (ΔE_{POL}, Figure 5B) stabilizes borane carbonyl only slightly more than ammonia borane. As a result, the stabilization due to the non-charge-transfer interactions ($\Delta E_{FRZ} + \Delta E_{POL}$, Figure 5C) is greater for H_3B-NH_3 than for H_3B-CO. The charge-transfer effects are drastically different in H_3B-CO and H_3B-NH_3: although the energy lowerings due to the electron donation to BH_3 are almost the same (Figure 5D), the stabilization due to back-donation effects is strong for borane carbonyl and only barely noticeable for ammonia borane (Figure 5E). Thus, the interplay between the energy components results in the same total interaction energy in H_3B-CO and H_3B-NH_3 although the true bonding mechanisms are far from being similar. Another indirect indication of different binding in these two complexes is the intermolecular distance − the B−N bond is 0.14 Å longer than the B−C bond (Table 2).

Despite the fact that complexes H_3B-CO, H_3B-N_2, and H_3B-CN^- are isoelectronic they have different stability and properties. EDA can be utilized to reveal the origin of these differences. As shown in Figure 5A, ΔE_{FRZ} components are very similar for N_2 and CO ligands. In the case of the charged H_3B-CN^- complex, polarization effects are substantially stronger than in the case of neutral complexes (Figure 5B) and H_3 B−CN^- is significantly stabilized just by polarization (Figure 5C). Comparison of the charge-transfer curves for the three complexes (Figures 5D and 5E) leads to the well-known conclusion that CO is a strong, well balanced σ-donor and π-acceptor, N_2 is a weaker balanced σ -donor and π-acceptor, whereas CN^- is a very good σ-donor but a very poor π-acceptor. Geometrical distortion of the BH_3 unit is noticeable in these complexes, whereas distortion of the diatomic molecule is insignificant. The BH_3 distortion is the highest for CN^- most likely because of its high polarizing power. N_2 causes the least geometrical changes in BH_3.

As a result of strong polarization and σ-donation effects, CN^- forms very strong bonds with BH_3. Polarization strength of the CO ligand is lower, but it is partially compensated by its good π-electron accepting properties. Therefore, binding in H_3B-

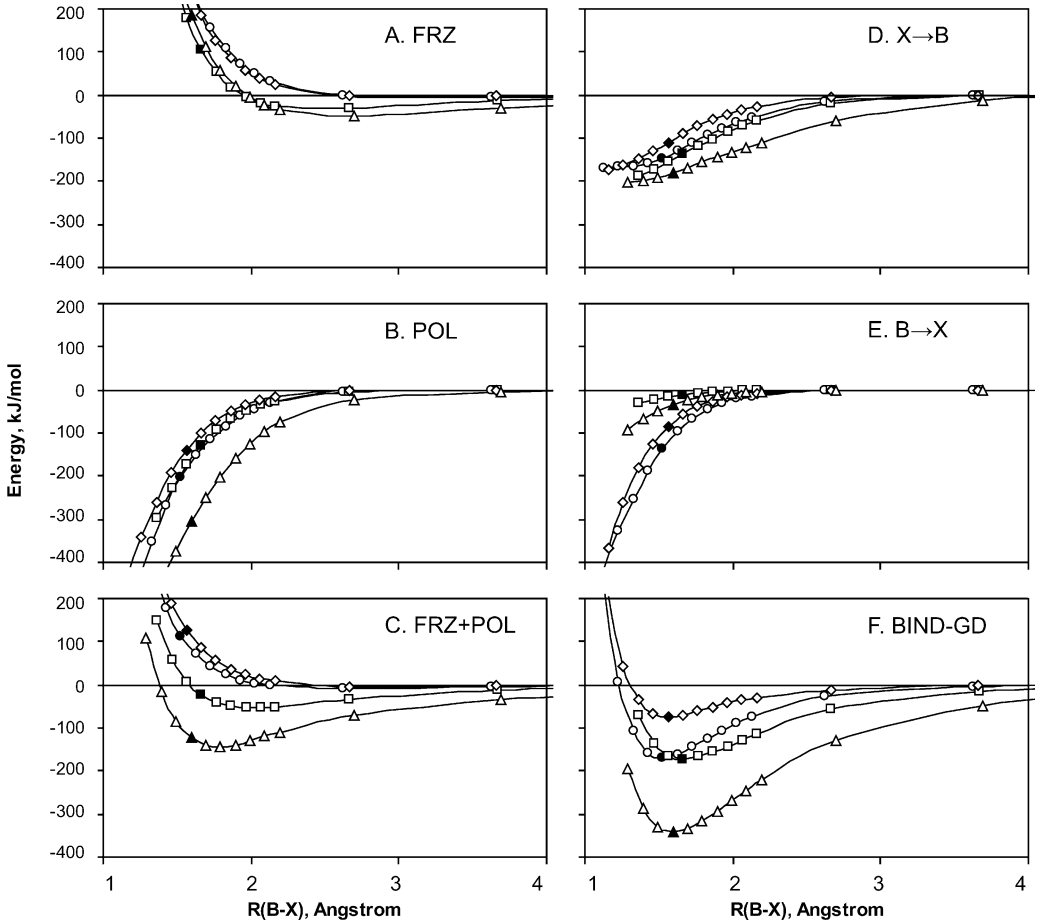

Figure 5. Dependence of the energy components on the distance between the monomers in borane adducts: H_3B-NH_3 (□); H_3B-CO (○); H_3B-N_2 (◇); H_3B-CN^- (△). Filled points on the curves correspond to the B3LYP/6-31(+,+)G(d,p) equilibrium geometries.

CO is not as strong as in H_3B-CN^-, but it is still approximately 85 kJ/mol stronger than binding in H_3B-N_2.

3.4. Synergic Bonding in Pt−Alkene Complexes. The metal−alkene bonding in Zeise's salt and its analogs is a classic example of the Dewar−Chatt−Duncanson model of synergic bonding between a double bond and a metal.[78−80] According to this model, the alkene donates the electron density from its π-bonding orbital into the metal unoccupied orbitals, and the metal donates the electron density back from its occupied orbitals into the carbon−carbon π-antibonding orbital. This conceptual description is widely accepted in organometallic chemistry and allows one to make qualitative prediction of properties of metal complexes based on the classification of ligands in terms of the strength of forward-donation and back-bonding interactions.[81] Description of the synergic interactions in metal−alkene complexes can in principle be made quantitative with energy partitioning methods.[82−84] In this section, we analyze bonding in Zeise's salt $[Cl_3Pt(\eta^2\text{-}C_2H_4)]^-$ and its analogs in which the Cl^- ligands are replaced with F^- and Br^-.

Complex geometries were optimized using the BP86 density functional with the effective core potential LANL2DZ basis for the Pt atoms and the 6-31(+,+)G(d,p) basis for all other atoms. The EDA calculations are also done at the BP86/LANL2DZ/6-31(+,+)G(d,p) level, and the results are summarized in Table 3.

In all three complexes, the frozen density interactions are repulsive, polarization effects are not large (15−20% of the total favorable binding), and as expected, the charge transfer is the major force that stabilizes the metal−alkene bond. These strong charge-transfer effects can be reproduced by single Roothaan step reasonably well; ΔE_{CT}^{HO} is around 10% of the variational charge-transfer energy. Unlike charge-transfer effects in classical donor−acceptor complexes like $Na(H_2O)_4^+$ or H_3B-NH_3 (Figure 4 and Table 2), charge transfer in Zeise's salt calculated with ALMO EDA occurs both ways: from the ligand to the metal and from the metal to the ligand. The stabilization energies of forward donation and back-bonding effects in $[Cl_3Pt(\eta^2\text{-}C_2H_4)]^-$ are approximately equal and, thus, correctly reproduce the qualitative description of the Dewar−Chatt−Duncanson model. A pictorial representation of the orbital interactions corresponding to forward donation and back-bonding is given in Figure 6.

TABLE 3: B3LYP/LANL2DZ/6-31(+,+)G(d,p) EDA Results (kJ/mol) for $[X_3Pt(\eta^2\text{-}C_2H_4)]^-$

	X		
	F	Cl	Br
ΔE_{FRZ}	241	238	247
ΔE_{POL}	−67	−74	−76
$\Delta E^{RS}_{X_3Pt\rightarrow C_2H_4}$	−211	−158	−156
$\Delta E^{RS}_{C_2H_4\rightarrow X_3Pt}$	−146	−144	−138
ΔE_{CT}^{HO}	−33	−36	−34
$\Delta E_{GD}(X_3Pt)$	8	14	16
$\Delta E_{GD}(C_2H_4)$	31	26	26
ΔE_{BIND}	**−178**	**−134**	**−115**
ΔE_{BSSE}	7	7	12
ΔE^{RS}_{BSSE}	7	7	11
d(C−Pt), Å	2.12	2.16	2.18
d(X−H), Å	2.70	2.90	2.97

One can see from Table 3 that ΔE_{FRZ} terms do not differ by more than 9 kJ/mol when the halogen ligands are changed. The

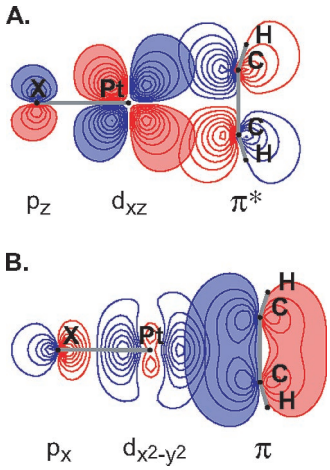

Figure 6. Pictorial representation of the orbital interactions in $[X_3Pt(\eta^2\text{-}C_2H_4)]^-$: (A) back-bonding; (B) forward donation. Filled contours represent occupied orbitals; unfilled contours represent unoccupied orbitals.

same can be said about ΔE_{POL}: the spread is 9 kJ/mol for F^-, Cl^-, and Br^- ligands. There is only a small difference in the charge-transfer energy between Br^- and Cl^-, but ΔE_{CT} for F^- is 50 kJ/mol lower than for Br^- and Cl^-. Analysis of the charge-transfer term shows that it is the back-bonding component that is responsible for this difference whereas the forward donation terms are nearly the same for the F^-, Cl^-, and Br^- ligands. The origin of this effect can be understood by a detailed examination of the orbital interactions in the complex. The occupied orbital of the $[X_3Pt]^-$ fragment that donates electrons to the unoccupied π^* orbital of ethene is the antibonding orbital formed upon interaction of the $5d_{xz}$ orbital on Pt and the valence p_z orbital on one of the X^- ligands. This occupied antibonding orbital is shown in Figure 6A. Because the $2p_z$ orbital of F^- lies closer in energy to the $5d_{xz}$ orbital on Pt than to the $3p_z$ orbital of Cl^- the resulting antibonding orbital lies higher in energy in the $[F_3Pt]^-$ complex than in the $[Cl_3Pt]^-$ complex and, therefore, gives stronger interaction with the high-energy π^* ethene orbital.

3.5. Interaction of Molecular Hydrogen with Transition Metal Centers. Molecular hydrogen is considered to be a clean, renewable replacement for the world's diminishing fossil fuel resources. However, a conversion to a hydrogen-based economy is far from realization as present day technology is not capable of dealing with issues of effective fuel storage.[85,86] Developing viable hydrogen storage materials (HSMs) is thus a particular challenge. Microporous metal−organic frameworks (MOFs) are potential HSM candidates that consist of inorganic metal−oxide clusters bridged by organic linkers.[87−89] To improve the H_2 interaction with the framework it has been suggested to embed open/unsaturated metal sites within the organic linker because unsaturated or partially charged metal centers could have a tremendous effect on the H_2 binding affinity.[90−92]

There is experimental evidence to show that molecular hydrogen can coordinate with chromium to form stable σ-bonded H_2 complexes such as $(\eta^6\text{-}C_6H_6)Cr(H_2)(CO)_2$.[9,93] Therefore, it may be possible to synthesize hybrid MOFs where the $Cr(CO)_3$ groups are complexed to the aromatic organic linkers,[94,95] and subsequently, the CO ligands are removed to allow up to three H_2 molecules to interact with the resulting coordinatively unsaturated chromium complexes. Here we analyze the nature of the H_2 interaction with the chromium site in $(\eta^6\text{-}C_6H_6)Cr(H_2)_3$ complex (Figure 7A) and study the effect of simple π-electron-donating and π-electron-withdrawing substituents (R) in the benzene ring on the $Cr-H_2$ interaction energy.[96]

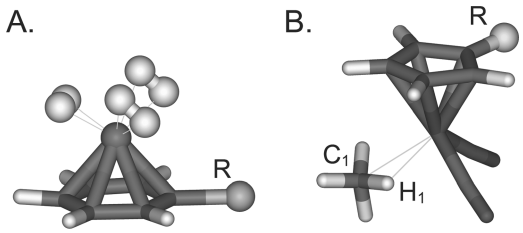

Figure 7. (A) $(R\text{-}C_6H_6)Cr(H_2)_3$ complex. (B) $(R\text{-}Cp)Re(CO)_2(CH_4)$ complex.

Geometry optimization and EDA of the binding energies were performed using BP86 density functional theory with the SRSC effective core potential basis for the Cr atoms and the 6-311G-(d,p) basis for the rest of the atoms. Each dihydrogen molecule represented a fragment. Results of the energy decomposition are shown in Figure 8 (see also Table S2 in the Supporting Information).

For visual clarity, the results of the EDA in Figure 8 are presented in the following way:

- A reference value is chosen for each energy component as the maximum value of this component in the series of substituted complexes: ΔE^{ref}_{FRZ}, ΔE^{ref}_{POL}, etc.
- The relative energy terms are calculated for each complex as a difference between the energy term and the corresponding reference value (e.g., $\Delta\Delta E_{FRZ} = \Delta E_{FRZ} - \Delta E^{ref}_{FRZ}$). The relative values are plotted on the graph.
- The reference values for each energy term are summed to give the total interaction energy for the reference complex (ΔE^{ref}_{BIND}) and the *Y*-axis of the graph is shifted by ΔE^{ref}_{BIND}.

Thus, the relative terms constructed in this way are always negative and their absolute values represent the stabilization energy of the component relative to the corresponding reference value. Also, the total length of the column in the graph represents the overall stabilization of the complex relative to ΔE^{ref}_{BIND}. The shift of the *Y*-axis ensures that the position of the lower edge of the column gives the total interaction energy ΔE_{BIND}.

In addition to Figure 8, the absolute values of all energy components for all complexes are included in the Supporting Information in Table S2.

For all H_2 complexes, the frozen density interactions are repulsive. Charge transfer is the dominant contribution to the binding between H_2 and the Cr center and amounts to 65−67% of the total favorable binding contributions. The polarization effects contribute the remaining 33−35%. The forward donation energy (from H_2 to the metal) is higher in magnitude (around −90 kJ/mol) than the back-donation energy (between −52 and −81 kJ/mol); however, the energy of charge transfer between neighboring hydrogen molecules as well as higher order relaxation effects are negligibly small (few kJ/mol).

It can be seen from Figure 8 that the frozen density and the polarization energy terms are strongly affected by the substituent on benzene. The spread in ΔE_{FRZ} values is 42 kJ/mol, and the spread in ΔE_{POL} values is 41 kJ/mol. However, there is apparent correlation between ΔE_{FRZ} and ΔE_{POL} terms: high positive values of ΔE_{FRZ} correspond to large negative values of ΔE_{POL}, and therefore, the sum of their relative contributions (Figure 8) is not that strongly influenced by the benzene substituents (the spread is decreased to 19 kJ/mol). The combined stabilization due to the non-charge-transfer effect is generally smaller for electron-withdrawing groups.

The forward donation energy is insensitive to the nature of the substituent in the benzene ring (the spread is 8 kJ/mol), whereas back-donation is more pronounced for π-electron-

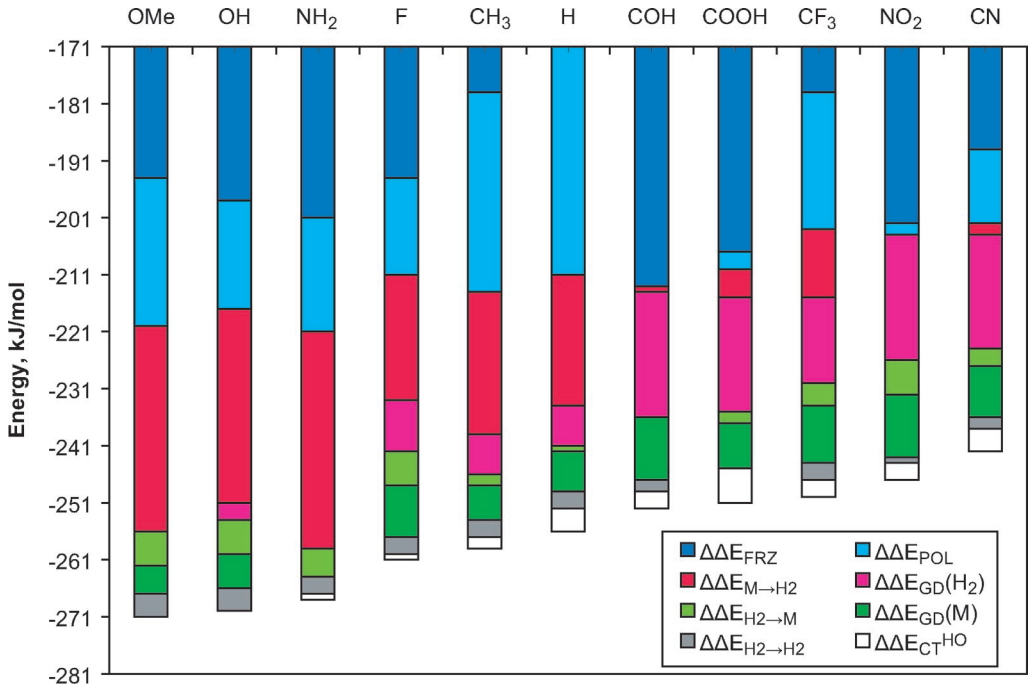

Figure 8. BP86/SRSC/6-311G(d,p) EDA results for (R-C_6H_5)Cr(H_2)$_3$ complexes. On the vertical axis are the (negative semi-definite) differences in each component of the energy decomposition relative to the reference value, which is defined as the maximum of that component overall substituents. Each different phenyl substituent, R, is marked across the top of the plot. See text for further details. Reference values for the energy components, kJ/mol: $\Delta E^{ref}_{FRZ} = 349$, $\Delta E^{ref}_{POL} = -209$, $\Delta E^{ref}_{M\rightarrow H2} = -166$, $\Delta E^{ref}_{GD}(H_2) = 77$, $\Delta E^{ref}_{H2\rightarrow M} = -261$, $\Delta E^{ref}_{GD}(M) = 37$, $\Delta E^{ref}_{H_2\rightarrow H_2} = -11$, $\Delta E^{ref}_{HO} = 13$, $\Delta E^{ref}_{BIND} = -171$.

donating groups (maximum absolute value is 81 kJ/mol) and is less pronounced for π-electron-withdrawing groups (maximum absolute value is 52 kJ/mol). This trend can be rationalized as follows: π-electron-withdrawing substituents decrease the electron density on benzene, which in turn pulls the electrons from the metal thus decreasing the electron density flow from the metal to the hydrogen molecules.

The trend observed for the back-donation energy is consistent with the trends in the calculated H−H bond lengths and the corresponding H_2 geometry relaxation terms. The higher the back-donation energy term, the longer the H−H distance is (Table S2 in the Supporting Information). In turn, the change in the H−H bond length with respect to its gas-phase value determines the $\Delta E_{GD}(H_2)$ term. Therefore, in the case of H_2 binding, $\Delta E_{GD}(H_2)$ can be combined with the back-donation energy term to emphasize that charge transfer to the antibonding orbitals of H_2 is indeed the driving force for the geometric distortion of H_2. The correlation of these two terms is apparent from Figure 8. The combined term, $\Delta\Delta E_{H_2\rightarrow M} + \Delta\Delta E_{GD}(H_2)$, does not vary as much as the back-bonding term alone (its spread is 16 kJ/mol).

On the basis of the EDA results, we conclude that there exists a correlation between the electronic effects of the substituents (both strength and direction) and the amount of charge transfer from Cr to H_2. The combined frozen density and polarization term is also correlated with the substituent effects. The calculated binding energies indicate that the π-electron-donating substituents (R = OCH_3, OH, NH_2, F, CH_3) increase the H_2 binding to the metal center relative to the parent complex (R = H) and the π-electron-withdrawing groups (R = COH, COOH, CF_3, NO_2, CN) decrease it. In terms of magnitude, the effect is not significant (1−7% of the overall binding energies), but it could possibly be further enhanced in the presence of multiple electron-withdrawing groups. This example demonstrates how the energy decomposition analysis determines which factors might be used to tune the H_2 interaction strength. Such information could be used as input to optimize the design of hybrid MOFs.

3.6. Interaction of Methane with (η^6-C_5H_5)Re(CO)$_2$ Complex. Carbon−hydrogen bond activation reactions in alkanes are industrially important, as they could be used for the conversion of inexpensive inert alkanes into reactive molecules.[97,98] Transition metal complexes are known for their ability to activate C−H bonds in alkanes.[99] It is widely accepted that C−H activation reactions proceed via alkane σ-complex intermediates.[99] Such species have recently been detected and studied in low-temperature NMR experiments.[100,101] Although much of the effort has been devoted to isolation and structural characterization of intermolecular alkane C−H/metal complexes, these attempts have not been successful thus far.

Experimental studies of the reaction of CpM(CO)$_x$(*n*-heptane) complex with CO have found that the rate of displacement of *n*-heptane by CO decreases with the identity of M both across and down groups 5, 6, and 7 of the periodic table. For example, CpV(CO)$_3$(*n*-heptane) reactes with CO 50 000 times more rapidly than CpRe(CO)$_2$(*n*-heptane).[102,103] In agreement with the observed trends, several rhenium complexes with large alkanes have now been detected using low-temperature NMR.[100,101] In this section we apply the ALMO EDA to study the factors contributing to the stability of σ-complexes of methane with substituted cyclopentadienyl-dicarbonyl-rhenium(I) complexes (R-Cp)Re(CO)$_{2-x}$(L)$_x$(CH_4).[104]

Geometry optimization of the complexes and the EDA were again performed using the BP86 functional with the LANL2DZ effective core potential basis for the Re atoms and the 6-31(+,+)G(d,p) basis for all other atoms. In the final structure, the substituent in the Cp ring is oriented away from the methane ligand, which has a C−H bond coordinated to the Re atom (Figure 7B). Results of the energy decomposition are shown in Figure 9 (see also Table S3 in the Supporting Information). The meaning of the terms in Figure 9 is the same as that in Figure 8.

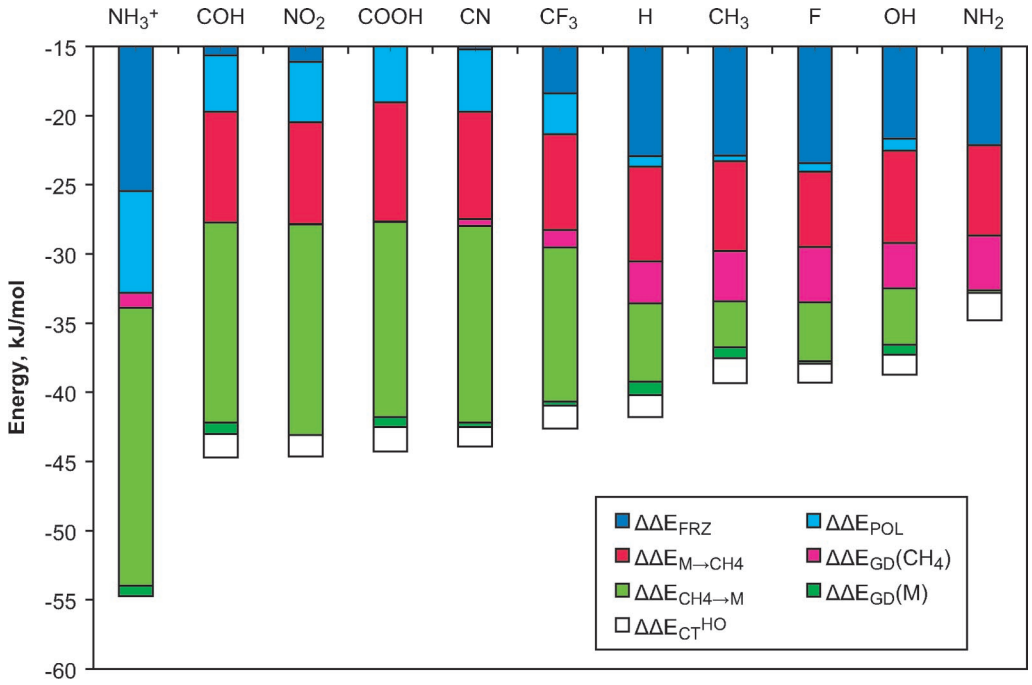

Figure 9. BP86/LANL2DZ/6-31(+,+)G(d,p) EDA results for the (R-Cp)Re(CO)$_2$(CH$_4$) complexes. See the caption of Figure 8 and the text for full description of the quantities plotted. Reference values for the energy components, kJ/mol: $\Delta E^{ref}_{FRZ} = 74$, $\Delta E^{ref}_{POL} = -26$, $\Delta E^{ref}_{M\rightarrow CH_4} = -21$, $\Delta E^{ref}_{GD}(CH_4) = 17$, $\Delta E^{ref}_{CH_4\rightarrow M} = -67$, $\Delta E^{ref}_{GD}(M) = 3$, $\Delta E^{ref}_{HO} = 6$, $\Delta E^{ref}_{BIND} = -15$.

TABLE 4: BP86/LANL2DZ/6-31(+,+)G(d,p) EDA Results (kJ/mol) for the (Cp)Re(CO)(L)(CH$_4$) Complexes

	L				
	NO^+	CO	N_2	CN^-	NH_3
ΔE_{FRZ}	68	66	52	61	50
ΔE_{POL}	−42	−27	−23	−22	−19
$\Delta E^{RS}_{M\rightarrow CH_4}$	−19	−28	−20	−28	−24
$\Delta E^{RS}_{CH_4\rightarrow M}$	−100	−73	−55	−38	−36
ΔE^{HO}_{CT}	8	4	6	4	5
$\Delta E_{GD}(M)$	3	2	2	9	21
$\Delta E_{GD}(CH_4)$	18	14	10	8	5
ΔE_{BIND}	**−65**	**−42**	**−28**	**−7**	**2**
ΔE_{BSSE}	5	4	4	3	4
ΔE^{RS}_{BSSE}	5	4	4	3	4
$d(C_1-H_1)$, Å[a]	1.164	1.160	1.151	1.155	1.142
$d(Re-H_1)$, Å	1.933	1.935	1.957	1.994	2.018
$d(Re-C_1)$, Å	2.642	2.635	2.670	2.812	2.840

[a] $d(C_1-H_1) = 1.101$ Å in the uncoordinated methane molecule.

The ALMO EDA for the unsubstituted CpRe(CO)$_2$(CH$_4$) shows that the major contribution to binding between methane and Re is due to charge transfer (78% of the total favorable binding contributions, ΔE_{POL} and ΔE_{CT}), whereas polarization is less significant (22%) and the frozen density interaction is repulsive (Table 4). A majority (72%) of ΔE_{CT} is associated with charge transfer from the occupied orbitals of alkane to the vacant orbitals of the metal complex, and the remainder is due to back-bonding (ΔE^{HO}_{CT} is less than 5% of the overall charge-transfer term). The goal in designing an isolable σ-complex should be to choose the combination of ligands that is the most thermodynamically stable with respect to reactants and yet also has a high barrier to oxidative addition. Therefore, it is desirable to increase the binding energy of methane without increasing the charge transfer from the metal complex to methane because a strong back-bonding will result in cleavage of the C−H bond. As seen from Figure 9, placing π-electron-withdrawing groups into the Cp ring increases the forward donation of electron density from methane to the metal and, thus, increases the overall binding energy. The back-bonding term is insensitive to the Cp ring substitution. The π-electron-donating groups have the opposite effect and destabilize the σ-complex.

The magnitude of the substituent effect is not very strong. The overall binding energy in the most stable σ-complex (R = NO_2) is increased only by 3 kJ/mol (7%) relative to the unsubstituted CpRe(CO)$_2$(CH$_4$) complex. Although this stabilization itself is not enough to make the σ-complex isolable, increasing the number and the strength of π-electron-withdrawing groups in the Cp ring will assist in design of a stable alkane σ -complex. For example, in a hypothetical positively charged complex with a strong electron-withdrawing NH_3^+ group in the Cp ring, the binding energy is increased by 13 kJ/mol (31%) relative to CpRe(CO)$_2$(CH$_4$) (some stabilization comes from non-charge-transfer effects).

Placing electron-withdrawing groups closer to the metal center (i.e., replacing CO ligands with stronger π-acceptors) can also lead to stronger binding of methane on Re. Indeed, in the series of isoelectronic ligands, NO^+, CO, N_2, CN^-, the strongest methane binding is observed for the strongest π -acceptor, NO^+ (Table 4). The EDA shows that the increase in the binding energy is due to increased forward donation and polarization. For the NO^+ ligand, methane binding is 23 kJ/mol (or 55%) stronger than that for CO.

Using large ligands instead of CO will decrease the relative stability of the σ-complexes because of sterical constraints around the rhenium atom. As seen from Table 4, geometry distortion effects are large even for the relatively small NH_3 ligand, and although the σ-complex is a true minimum on the energy surface, it is energetically less stable than the isolated methane and CpRe(CO)(NH_3)(CH$_4$) molecules ($\Delta E_{BIND} > 0$).

Overall, we conclude that the ALMO EDA can be used to explain the nature of the alkane−metal interaction in σ-complexes and to make computational predictions of the relative

stabilities of these complexes as a function of substituent. Small electron deficient ligands lead to the strongest alkane-metal binding.

4. Conclusions

In this paper we have presented an energy decomposition analysis (EDA) method based on absolutely localized molecular orbitals (ALMO). The ALMO EDA enables accurate separation of the total intermolecular interaction energy into frozen density, polarization, and charge-transfer energy terms. The newly proposed method has been tested successfully on systems involving hydrogen bonding, donor−acceptor interaction, and both π- and σ-complexes. For well understood cases such as the water dimer, H_3B-NH_3, and Zeise's anion the ALMO EDA results are broadly consistent with existing understanding of intermolecular bonding. Additionally, we have demonstrated that the ALMO EDA can be used to assist in solving practical chemical problems such as tuning metal−H_2 and metal−alkane binding strength. The main advantages of the ALMO EDA follow:

1. All terms are calculated variationally and the method is applicable to weakly and strongly interacting molecular systems.
2. The charge-transfer energy can be further decomposed into forward donation and back-bonding contributions, associated with a single Roothaan step plus generally small higher order charge-transfer energy lowering that cannot be readily decomposed.
3. Basis set superposition error in the charge-transfer term can be corrected for both variational and Roothaan step calculations.
4. From the computational viewpoint, the ALMO EDA is very fast and can be applied to systems of hundreds of molecules at a cost comparable to the cost of regular SCF single point calculations.

The primary limitation of the ALMO EDA at present is the need to have physically well-defined fragments each with an integer number of electrons. This requirement distinguishes intermolecular from intramolecular interactions. A secondary limitation is that we have defined the ALMO EDA only for single determinant wavefunctions so far. This is a limitation we hope to lift in the future.

Acknowledgment. This work was supported by the Director, Office of Basic Energy Sciences, Chemical Sciences Division of the U.S. Department of Energy under contract DE-AC03-76SF00098 and by the National Science Foundation under grant CHE-0535710. Additional support for hydrogen binding calculations was provided by the Department of Energy through grant no. DE-FG36-05GO15002.

5. Appendix: Mathematical and Computational Details of the ALMO EDA

The following indices are used throughout: *x*, *y*, *z* are the molecule (fragment) indices, *i*, *j* are the occupied MO indices, *a*, *b* are virtual MO indices. Tensor notation[105] is used to work with the nonorthogonal basis sets with one exception, which is that the Einstein convention does not imply summation over molecule indices.[43]

Relaxation of the occupied ALMOs is performed using the locally projected SCF method of Gianinetti et al.[43,46] as implemented in the Q-Chem software package.[48] In addition to the occupied ALMOs, this method yields a set of nonredundant linearly independent virtual ALMOs. After the locally projected equations are converged, the occupied subspace is projected out from the virtual ALMOs that span the virtual subspace to ensure strong orthogonality of the subspaces. The Roothaan step BSSE-corrected energy lowering in eq 6 is a quasi-perturbative energy correction[43,106,107] that can be expressed as

$$\Delta E_{CT}^{RS} = \sum_{x,y} F^{xi}{}_{ya} t^{ya}{}_{xi} + \Delta E_{BSSE}^{RS} \quad (7)$$

where $F^{xi}{}_{ya}$ is the ALMO contravariant−covariant representation of the Fock operator build from the converged ALMO wavefunction (Ψ_{ALMO}), and $t^{ya}{}_{xi}$ is the amplitude corresponding to electron excitation (transfer) from the converged absolutely localized occupied orbital *i* on fragment *x* to the virtual orbital *a* on fragment *y*. Therefore, the energy of the electron transfer from fragment *x* to fragment *y* in eq 6 is expressed as

$$\Delta E_{x\rightarrow y}^{RS} = F^{xi}{}_{ya} t^{ya}{}_{xi} + \Delta E_{BSSE(x\rightarrow y)}^{RS} \quad (8)$$

The variational nature of the polarized ALMOs guarantees that the delocalization energy term within a molecule is zero, $F^{xi}{}_{xa} t^{xa}{}_{xi} = 0$.

The BSSE correction terms $\Delta E_{BSSE(x\rightarrow y)}^{RS}$ in eq 8 are also calculated using the single Roothaan step counterpoise method instead of conventional iterative variational counterpoise correction.[49] In the case of the RS counterpoise correction the indices in eqs 7 and 8 refer to the MO orbitals of isolated monomers, not to the converged ALMOs from the SCF MI calculations. Another difference is that all occupied orbitals are localized on one molecule, and all orbitals on the other molecules are virtual ghost orbitals. For all systems in this paper, the difference between the Roothaan step counterpoise correction, ΔE_{BSSE}^{RS}, and the variational correction, ΔE_{BSSE}, is less than 0.3 kJ/mol.

Equation 7 can also in principle be used to perform a more detailed orbital interaction analysis. In this case the energy of charge transfer from the occupied orbital *i* on fragment *x* to the virtual orbital *a* on fragment *y* is simply $F^{xi}{}_{ya}$ multiplied by the corresponding amplitude $t^{ya}{}_{xi}$ (no summation over the orbital indices).

The amplitudes $t^{ya}{}_{xi}$ can be found by solving the Roothaan step quadratic equation:[107]

$$F^{zb}{}_{xi} + \sum_{y} F^{zb}{}_{ya} t^{ya}{}_{xi} - \sum_{y} t^{zb}{}_{yj} F^{yj}{}_{xi} - \sum_{y,z} t^{zb}{}_{yj} F^{yj}{}_{za} t^{za}{}_{xi} = 0 \quad (9)$$

In practice, the linearized version of the amplitude equation, with the last term neglected, is solved in the symmetrically orthogonalized ALMO representation by the preconditioned conjugate gradient method. Then the solution of the linearized equation is used as an initial guess to solve quadratic eq 9 using the Newton method. Finally, the amplitudes are transformed back to the ALMO representation.

If the amplitudes obtained from the linearized equation are used to calculate ΔE_{CT}^{RS}, then the energy lowering is equivalent to the second-order single excitation perturbation theory result.[43,106] If the amplitudes are obtained from quadratic eq 9, then the energy lowering is equvalent to the result of single Fock matrix diagonalization or infinite-order single excitation perturbation theory result.[43,106] We used the quadratic equation to calculate amplitudes and ΔE_{CT}^{RS} for all systems in this paper.

Special care must be taken of the grid superposition error (GSE) when calculating the interaction energies with DFT. An atom-centered finite quadrature grid is used in the density functional calculations to compute complicated integrals in the exchange-correlation functionals that cannot be evaluated

analytically.[108,109] Therefore, if the finite grid associated with a molecule is not large enough, then addition of the grid points of another molecule can change the energy of the first molecule even if the second molecule has no basis functions, nuclei, or electrons. This is a spurious effect and does not represent any physical interactions. The counterpoise calculations correct the charge-transfer term for both GSE and BSSE. However, in this work, we did not attempt to separate the GSE into the forward donation and the back-bonding components ($\Delta E^{RS}_{GSE(x\rightarrow y)}$). Instead, large grids were used to make GSE negligibly small.

Supporting Information Available: Tabular representation of Figures 4, 8, and 9. This material is available free of charge via the Internet at http://pubs.acs.org.

References and Notes

(1) Lehn, J.-M. *Supramolecular Chemistry: Concepts and Perspectives*; Weinheim: New York, 1995.

(2) Steed, J. W.; Atwood, J. L. *Supramolecular Chemistry*; Wiley: New York, 2000.

(3) Desiraju, G.; Steiner, T. *The Weak Hydrogen Bond in Structural Chemistry and Biology*; Oxford University Press: New York, 1999.

(4) Jeffrey, G. A. *An Introduction to Hydrogen Bonding*; Oxford University Press: Oxford, U.K., 1997.

(5) Scheiner, S. *Hydrogen Bonding: A Theoretical Perspective*; Oxford University Press: Oxford, U.K., 1997.

(6) Wilkinson, G., Gillard, R., McCleverty, J., Eds. *Comprehensive coordination chemistry: the synthesis, reactions, properties, and applications of coordination compounds*; Pergamon Press: New York, 1987.

(7) Jean, Y. *Molecular orbitals of transition metal complexes*; Oxford University Press: Oxford, U.K., 2005.

(8) Shilov, A. E. *Metal complexes in biomimetic chemical reactions : N_2 fixation in solution, activation, and oxidation of alkanes, chemical models of photosynthesis*; CRC Press: Boca Raton, New York, 1997.

(9) Kubas, G. J. *Metal dihydrogen and σ-bond complexes: structure, theory and reactivity*; Kluwer Academic: New York, 2002.

(10) Van Leeuwen, P., Morokuma, K., Van Lenthe, J. H., Eds. *Theoretical aspects of homogeneous catalysis: applications of ab initio molecular orbital theory*; Kluwer Academic: Boston, 1995.

(11) Stone, A. J. *The theory of intermolecular forces*; Oxford University Press: New York, 1996.

(12) Jeziorski, B.; Moszynski, R.; Szalewicz, K. *Chem. Rev.* **1994**, *94* (7), 1887−1930.

(13) Moszynski, R.; Heijmen, T. G. A.; Jeziorski, B. *Mol. Phys.* **1996**, *88* (3), 741−758.

(14) Kitaura, K.; Morokuma, K. *Int. J. Quantum Chem.* **1976**, *10* (2), 325−340.

(15) Stevens, W. J.; Fink, W. H. *Chem. Phys. Lett.* **1987**, *139* (1), 15−22.

(16) Chen, W.; Gordon, M. S. *J. Phys. Chem.* **1996**, *100* (34), 14316−14328.

(17) Bagus, P. S.; Hermann, K.; Bauschlicher, C. W. *J. Chem. Phys.* **1984**, *80* (9), 4378−4386.

(18) Bagus, P. S.; Illas, F. *J. Chem. Phys.* **1992**, *96* (12), 8962−8970.

(19) Glendening, E. D.; Streitwieser, A. *J. Chem. Phys.* **1994**, *100* (4), 2900−2909.

(20) Schenter, G. K.; Glendening, E. D. *J. Phys. Chem.* **1996**, *100* (43), 17152−17156.

(21) Glendening, E. D. *J. Phys. Chem. A* **2005**, *109* (51), 11936−11940.

(22) Mochizuki, Y.; Fukuzawa, K.; Kato, A.; Tanaka, S.; Kitaura, K.; Nakano, T. *Chem. Phys. Lett.* **2005**, *410* (4−6), 247−253.

(23) Korchowiec, J.; Uchimaru, T. *J. Chem. Phys.* **2000**, *112* (4), 1623−1633.

(24) van der Vaart, A.; Merz, K. M. *J. Phys. Chem. A* **1999**, *103* (17), 3321−3329.

(25) Curutchet, C.; Bofill, J. M.; Hernandez, B.; Orozco, M.; Luque, F. J. *J. Comput. Chem.* **2003**, *24* (10), 1263−1275.

(26) Piquemal, J. P.; Perera, L.; Cisneros, G. A.; Ren, P. Y.; Pedersen, L. G.; Darden, T. A. *J. Chem. Phys.* **2006**, *125* (5), 054511.

(27) Rafat, M.; Popelier, P. L. A. *J. Comput. Chem.* **2007**, *28* (1), 292−301.

(28) Cisneros, G. A.; Piquemal, J. P.; Darden, T. A. *J. Chem. Phys.* **2006**, *125* (18), 184101.

(29) Piquemal, J. P.; Cisneros, G. A.; Reinhardt, P.; Gresh, N.; Darden, T. A. *J. Chem. Phys.* **2006**, *124* (10), 104101.

(30) Ponder, J. W.; Case, D. A. *Protein Simulations*; Advances in Protein Chemistry Vol. 66; Academic Press: New York, 2003; pp 27−85.

(31) Halgren, T. A.; Damm, W. *Curr. Opin. Struct. Biol.* **2001**, *11* (2), 236−242.

(32) Gresh, N. *J. Chim. Phys. Phys.-Chim. Biol.* **1997**, *94* (7−8), 1365−1416.

(33) Misquitta, A. J.; Jeziorski, B.; Szalewicz, K. *Phys. Rev. Lett.* **2003**, *91* (3).

(34) Hesselmann, A.; Jansen, G. *Chem. Phys. Lett.* **2003**, *367* (5−6), 778−784.

(35) Gutowski, M.; Piela, L. *Mol. Phys.* **1988**, *64* (2), 337−355.

(36) Frey, R. F.; Davidson, E. R. *J. Chem. Phys.* **1989**, *90* (10), 5555−5562.

(37) Cybulski, S. M.; Scheiner, S. *Chem. Phys. Lett.* **1990**, *166* (1), 57−64.

(38) Cammi, R.; Bonaccorsi, R.; Tomasi, J. *Theor. Chim. Acta* **1985**, *68* (4), 271−283.

(39) Cammi, R.; Tomasi, J. *Theor. Chim. Acta* **1986**, *69* (1), 11−22.

(40) Ghanty, T. K.; Ghosh, S. K. *J. Phys. Chem. A* **2003**, *107* (36), 7062−7067.

(41) Liu, T.; Zhu, W. L.; Gu, J. D.; Shen, J. H.; Luo, X. M.; Chen, G.; Puah, C. M.; Silman, I.; Chen, K. X.; Sussman, J. L.; Jiang, H. L. *J. Phys. Chem. A* **2004**, *108* (43), 9400−9405.

(42) Pavelka, M.; Burda, J. V. *Chem. Phys.* **2005**, *312* (1−3), 193−204.

(43) Khaliullin, R. Z.; Head-Gordon, M.; Bell, A. T. *J. Chem. Phys.* **2006**, *124* (20), 204105.

(44) Stoll, H.; Wagenblast, G.; Preuss, H. *Theor. Chim. Acta* **1980**, *57* (2), 169−178.

(45) Cullen, J. M. *Int. J. Quantum Chem., Quantum Chem. Symp.* **1991**, *25*, 193−212.

(46) Gianinetti, E.; Raimondi, M.; Tornaghi, E. *Int. J. Quantum Chem.* **1996**, *60* (1), 157−166.

(47) Nagata, T.; Takahashi, O.; Saito, K.; Iwata, S. *J. Chem. Phys.* **2001**, *115* (8), 3553−3560.

(48) Shao, Y.; Molnar, L. F.; Jung, Y.; Kussmann, J.; Ochsenfeld, C.; Brown, S. T.; Gilbert, A. T. B.; Slipchenko, L. V.; Levchenko, S. V.; O'Neill, D. P.; DiStasio, R. A.; Lochan, R. C.; Wang, T.; Beran, G. J. O.; Besley, N. A.; Herbert, J. M.; Lin, C. Y.; Van Voorhis, T.; Chien, S. H.; Sodt, A.; Steele, R. P.; Rassolov, V. A.; Maslen, P. E.; Korambath, P. P.; Adamson, R. D.; Austin, B.; Baker, J.; Byrd, E. F. C.; Dachsel, H.; Doerksen, R. J.; Dreuw, A.; Dunietz, B. D.; Dutoi, A. D.; Furlani, T. R.; Gwaltney, S. R.; Heyden, A.; Hirata, S.; Hsu, C. P.; Kedziora, G.; Khalliulin, R. Z.; Klunzinger, P.; Lee, A. M.; Lee, M. S.; Liang, W.; Lotan, I.; Nair, N.; Peters, B.; Proynov, E. I.; Pieniazek, P. A.; Rhee, Y. M.; Ritchie, J.; Rosta, E.; Sherrill, C. D.; Simmonett, A. C.; Subotnik, J. E.; Woodcock, H. L.; Zhang, W.; Bell, A. T.; Chakraborty, A. K.; Chipman, D. M.; Keil, F. J.; Warshel, A.; Hehre, W. J.; Schaefer, H. F.; Kong, J.; Krylov, A. I.; Gill, P. M. W.; Head-Gordon, M. *Phys. Chem. Chem. Phys.* **2006**, *8* (27), 3172−3191.

(49) Boys, S. F.; Bernardi, F. *Mol. Phys.* **1970**, *19* (4), 553−566.

(50) Hamza, A.; Vibok, A.; Halasz, G. J.; Mayer, I. *J. Mol. Struct.: THEOCHEM* **2000**, *501*, 427−434.

(51) Nagata, T.; Iwata, S. *J. Chem. Phys.* **2004**, *120* (8), 3555−3562.

(52) Reed, A. E.; Curtiss, L. A.; Weinhold, F. *Chem. Rev.* **1988**, *88* (6), 899−926.

(53) Scheiner, S. *Annu. Rev. Phys. Chem.* **1994**, *45*, 23−56.

(54) Dyke, T. R.; Mack, K. M.; Muenter, J. S. *J. Chem. Phys.* **1977**, *66* (2), 498−510.

(55) Fellers, R. S.; Leforestier, C.; Braly, L. B.; Brown, M. G.; Saykally, R. J. *Science* **1999**, *284* (5416), 945−948.

(56) Liu, K.; Cruzan, J. D.; Saykally, R. J. *Science* **1996**, *271* (5251), 929−933.

(57) Keutsch, F. N.; Saykally, R. J. *Proc. Natl. Acad. Sci. U.S.A.* **2001**, *98* (19), 10533−10540.

(58) Isaacs, E. D.; Shukla, A.; Platzman, P. M.; Hamann, D. R.; Barbiellini, B.; Tulk, C. A. *Phys. Rev. Lett.* **1999**, *82* (3), 600−603.

(59) Ghanty, T. K.; Staroverov, V. N.; Koren, P. R.; Davidson, E. R. *J. Am. Chem. Soc.* **2000**, *122* (6), 1210−1214.

(60) Martin, T. W.; Derewenda, Z. S. *Nat. Struct. Biol.* **1999**, *6* (5), 403−406.

(61) Hellemans, A. *Science* **1999**, *283* (5402), 614−615.

(62) Rashin, A. A.; Topol, I. A.; Tawa, G. J.; Burt, S. K. *Chem. Phys. Lett.* **2001**, *335* (3−4), 327−333.

(63) Piquemal, J. P.; Marquez, A.; Parisel, O.; Giessner-Prettre, C. *J. Comput. Chem.* **2005**, *26* (10), 1052−1062.

(64) Cai, Z. L.; Sendt, K.; Reimers, J. R. *J. Chem. Phys.* **2002**, *117* (12), 5543−5549.

(65) Lau, Y. K.; Ikuta, S.; Kebarle, P. *J. Am. Chem. Soc.* **1982**, *104* (6), 1462−1469.

(66) Stace, A. *Science* **2001**, *294* (5545), 1292−1293.

(67) Subirana, J. A.; Soler-Lopez, M. *Annu. Rev. Biophys. Biomol. Struct.* **2003**, *32*, 27−45.

(68) Pearson, R. G. *J. Am. Chem. Soc.* **1963**, *85* (22), 3533−3543.

(69) Pearson, R. G. *Science* **1966**, *151* (3707), 172−177.

(70) Lewis, G. N. *J. Franklin Inst.* **1938**, *226*, 293.
(71) Finston, H. L.; Rychtman, A. C. *A New View of Current Acid-Base Theories*; John Wiley & Sons: New York, 1982.
(72) Lloyd, D. R.; Lynaugh, N. *J. Chem. Soc., Faraday Trans. 2* **1972**, *68* (6), 947−958.
(73) Beach, D. B.; Jolly, W. L. *Inorg. Chem.* **1985**, *24* (4), 567−570.
(74) Bauschlicher, C. W.; Ricca, A. *Chem. Phys. Lett.* **1995**, *237* (1−2), 14−19.
(75) Jonas, V.; Frenking, G.; Reetz, M. T. *J. Am. Chem. Soc.* **1994**, *116* (19), 8741−8753.
(76) Ermler, W. C.; Glasser, F. D.; Kern, C. W. *J. Am. Chem. Soc.* **1976**, *98* (13), 3799−3807.
(77) Erhardt, S.; Frenking, G. *Chem.−Eur. J.* **2006**, *12* (17), 4620−4629.
(78) Dewar, J. S. *Bull. Soc. Chim. Fr.* **1951**, *18* (3−4), C71−C79.
(79) Chatt, J.; Duncanson, L. A. *J. Chem. Soc.* **1953**, (Oct), 2939−2947.
(80) Frenking, G. *J. Organomet. Chem.* **2001**, *635* (1−2), 9−23.
(81) Elschenbroich, C.; Salzer, A. *Organometallics*; Wiley-VCH: Weinheim, 1992.
(82) Kim, C. K.; Lee, K. A.; Kim, C. K.; Lee, B. S.; Lee, H. W. *Chem. Phys. Lett.* **2004**, *391* (4−6), 321−324.
(83) Fornies, J.; Martin, A.; Martin, L. F.; Menjon, B. *Organometallics* **2005**, *24* (14), 3539−3546.
(84) Schwieger, S.; Wagner, C.; Bruhn, C.; Schmidt, H.; Steinborn, D. *Z. Anorg. Allg. Chem.* **2005**, *631* (13−14), 2696−2704.
(85) Coontz, R.; Hanson, B. *Science* **2004**, *305* (5686), 957−957.
(86) Schlapbach, L.; Zuttel, A. *Nature* **2001**, *414* (6861), 353−358.
(87) Rosi, N. L.; Eckert, J.; Eddaoudi, M.; Vodak, D. T.; Kim, J.; O'Keeffe, M.; Yaghi, O. M. *Science* **2003**, *300* (5622), 1127−1129.
(88) Rowsell, J. L. C.; Yaghi, O. M. *Angew. Chem., Int. Ed.* **2005**, *44* (30), 4670−4679.
(89) Rowsell, J. L. C.; Spencer, E. C.; Eckert, J.; Howard, J. A. K.; Yaghi, O. M. *Science* **2005**, *309* (5739), 1350−1354.
(90) Kitaura, R.; Onoyama, G.; Sakamoto, H.; Matsuda, R.; Noro, S.; Kitagawa, S. *Angew. Chem., Int. Ed.* **2004**, *43* (20), 2684−2687.
(91) Kitagawa, S.; Noro, S.; Nakamura, T. *Chem. Commun.* **2006**, *7*, 701−707.
(92) Ma, S. Q.; Zhou, H. C. *J. Am. Chem. Soc.* **2006**, *128* (36), 11734−11735.
(93) Goff, S. E. J.; Nolan, T. F.; George, M. W.; Poliakoff, M. *Organometallics* **1998**, *17* (13), 2730−2737.
(94) Hunter, A. D.; Shilliday, L.; Furey, W. S.; Zaworotko, M. J. *Organometallics* **1992**, *11* (4), 1550−1560.
(95) Hunter, A. D.; Mozol, V.; Tsai, S. D. *Organometallics* **1992**, *11* (6), 2251−2262.
(96) Lochan, R. C.; Khaliullin, R. Z.; Head-Gordon, M. Manuscript in preparation.
(97) Bergman, R. G. *Science* **1984**, *223* (4639), 902−908.
(98) Labinger, J. A.; Bercaw, J. E. *Nature* **2002**, *417* (6888), 507−514.
(99) Hall, C.; Perutz, R. N. *Chem. Rev.* **1996**, *96* (8), 3125−3146.
(100) Lawes, D. J.; Geftakis, S.; Ball, G. E. *J. Am. Chem. Soc.* **2005**, *127* (12), 4134−4135.
(101) Lawes, D. J.; Darwish, T. A.; Clark, T.; Harper, J. B.; Ball, G. E. *Angew. Chem., Int. Ed.* **2006**, *45* (27), 4486−4490.
(102) Childs, G. I.; Grills, D. C.; Sun, X. Z.; George, M. W. *Pure Appl. Chem.* **2001**, *73* (3), 443−447.
(103) Childs, G. I.; Colley, C. S.; Dyer, J.; Grills, D. C.; Sun, X. Z.; Yang, J. X.; George, M. W. *J. Chem. Soc., Dalton Trans.* **2000**, *12*, 1901−1906.
(104) Cobar, E. A.; Khaliullin, R. Z.; Bergman, R. G.; Head-Gordon, M. *Proc. Natl. Acad. Sci. U.S.A.* **2007**, *104* (17), 6963−6968.
(105) Head-Gordon, M.; Maslen, P. E.; White, C. A. *J. Chem. Phys.* **1998**, *108* (2), 616−625.
(106) Liang, W. Z.; Head-Gordon, M. *J. Phys. Chem. A* **2004**, *108* (15), 3206−3210.
(107) Liang, W. Z.; Head-Gordon, M. *J. Chem. Phys.* **2004**, *120* (22), 10379−10384.
(108) Chien, S. H.; Gill, P. M. W. *J. Comput. Chem.* **2006**, *27* (6), 730−739.
(109) Gill, P. M. W.; Johnson, B. G.; Pople, J. A. *Chem. Phys. Lett.* **1993**, *209* (5−6), 506−512.